Finite element analysis of high-speed catamaran structure in beam waves

Yuyang Zhang [1], Zhipeng Deng [2, *], Jinglei Yang [2]

[1] Ultra-high voltage Transmission Company, China Southern Power Grid Co., LTD., Haikou 46010, Hainan, China

[2] College of Marine Engineering, Jimei University, Xiamen 361021, Fujian, China

Abstract. In this work, the computational fluid dynamics (CFD) and finite element analysis (FEA) method was used to study the structural stresses of an aluminum alloy catamaran sailing at the speed of 10.5m/s in beam waves, to investigate the characteristics of stresses and deformations by one-way fluid-structure coupling method, and to perform the optimization of the hull structure by structural adjustments to the bow and stern. The results were as follows: The numerical method proposed in this paper was able to create an effective environment in beam wave and calculate the wave load. The wave load on the side facing the wave is much larger than that on the other side, and the deformation of the bow is larger than that of the stern. The maximum deformation at high speed is reduced by 46.45% by strengthening the transverse structure and lengthening the stiffener.

Keywords: High-speed catamaran; Finite element analysis (FEA); Beam wave; CFD; Stress deformation.

1. Introduction

In recent years, with the gradual improvement of ship performance requirements, high-performance ships have been developed rapidly. As a new type of ship different from conventional monohull ships, the catamaran is attracting more and more attention due to its good advantages in high-speed transportation, which has thin demihull structure and large deck area. Due to the double demihull structure, the transverse moment of inertia and righting moment are greater than in a monohull ship, so that the transverse stability and maneuverability are better. The large transverse span makes deformation more complicated caused by wave loads. When the catamaran is traveling at high speed, the hull is subjected to a larger wave impact and has larger impact areas in beam waves than in head waves, which means that the draft of the left and right hulls is not equal, so this is a great test for the hull structure, especially for the cross-deck.

Yunbo Li and Zheng Fu [1] used the open-source CFD code OpenFOAM based on viscous flow theory to numerically predict the motions and forces of a trimaran sailing in beam waves, analyze the laws of motion and forces, and explore the effects of wave steepness and wave frequency on the rolling stability. The results showed that the force and motion amplitude of the trimaran increased with increasing wave steepness, leading to a deterioration in rolling stability. The wave frequency had little effect on the roll amplitude, but had a significant effect on the roll moment which exhibited greater nonlinearity characteristic in the high-frequency wave, resulting in a deterioration in motion stability. Zhouyuan Xu [2] studied the characteristics of wave load and flow field on the basis of a two-dimensional model, simulated the berthing process, and analyzed the effects of berthing speed during the berthing process. The results showed that in the beam wave, the rolling amplitude was the greatest, and it was the easiest to get the green wave. In the oblique wave, the yaw amplitude was the largest, the bow and stern were the place where the deck was easiest to get wet. In the head wave, the pitch amplitude is the largest, the bow was the place where the deck was easiest to get wet, but it was less severe than in the oblique wave. Jiong Chen and Qi Yang et al [3] selected a 147.5-metre-long deck cargo ship as the research object, carried out the transverse structure strength calculation of an intact compartment in the cargo area using the finite element method, taking into account the transverse wave load, and investigated the characteristics of transverse bending and overturning problems due to the waves hitting the side of the hull. Huailiang

Li and Wentai Yu et al [4] took two barges as research objects named "Ocean Oil 225" and "Ocean Oil 226", conducted experimental simulation of the installation of the floating support in beam waves, and investigated the motion response of the two barges and the upper block, as well as the force characteristics of the leg docking unit in the stage of readiness and docking. It was found that due to the shadowing effect and the swaying effects of the intermediate water, the roll amplitude of the barge on the side facing wave is always greater than that on the side facing away from wave in beam waves, which resulted in significant vertical and horizontal impact loads on the leg docking unit during the docking stage. Weiwei Lu and Shujun Li et al [5] calculated the mooring stability of tugboat in beam waves using dynamic mooring analysis software aNyMOOR TERMSIM, obtained the ship impact force, bollard force and ship motion response under conditions of normal use and extreme working, compared the impact energy with the calculation results of "rule of Load for Harbour Engineering", analyzed the provisions of domestic and foreign rules on the conditions of ship mooring and motion response for small ships, and provided the recommended standards for tugboats in terms of waves and motions.

Most of research on the ships' structural performance focuses on the force and displacement of fluid-solid coupling. Jianjun Tu and Feng Feng et al [6] established a one-way fluid-solid coupling simulation method and analytical procedure that took into consideration the three-dimensional wave loads, and evaluated the structure strength of the planing boat using ANSYS Workbench software and standard formula method. The comparison results showed that the structure check was more accurate and that the simulation method used in this work was able to study the load characteristics in different positions of the planing boat structure. Xiaojie Tian and Dashuai Xie et al [7] analyzed the fluid-solid coupling characteristics of a gas-liquid two-phase flow marine riser using ANSYS software, investigated how the riser's vibration modes changed in the presence and absence of fluid-solid coupling, and studied how fluid boundary conditions affected the riser's intrinsic frequency and formation. The findings had significant theoretical implications for marine risers' optimal design and dependability throughout operation. With a fully nonlinear coupling solver, Ying Tang and his team [8] proposed a completely nonlinear numerical method for the hydroelasticity problem of flexible ships. In order to accurately predict the structural strength of the ship and further improve the quality of ship design, Yajie Yun established a full ship model, evaluated the ship drag, flow field and the forces on the ship surface in the hog and sag condition using the one-way fluid-structure coupling method, and analyzed the whole ship structure strength. Zhou, Lei, Meng, Du, An et al [10-14] used a similar method to carry out numerical studies on the fan blade, ringsail, wheel, and propeller.

The above research results have proved the feasibility and reliability of using the fluid-structure coupling method to deal with the problem of structure strength and motion response in beam waves. Based on the aforementioned research, this paper developed a finite element model for a 12m high-speed aluminum alloy catamaran, calculated the static and dynamic pressures using Computational Fluid Dynamics (CFD) and Finite Element Analysis (FEA) methods, examined the structural stress characteristics under different beam wave conditions, and optimized frame in preliminary in combination with the "Code for Classification and Construction of Offshore High Speed Vessels, Version 2022" (hereinafter referred to as the "Code") [15].

2. Theory and methods of numerical computation

2.1 Numerical theory

The governing equation in this paper used the Reynolds-averaged Navier-Stokes equations which were widely used in engineering [16], i.e., the RANS equations:

$$\frac{\partial \rho}{\partial t}+\frac{\partial}{\partial x_i}(\rho u_i)=0$$

$$\frac{\partial(\rho u_i)}{\partial t}+\frac{\partial(\rho u_i u_i)}{\partial x_j}=-\frac{\partial p}{\partial x}+\frac{\partial}{\partial x_j}\left(\mu\frac{\partial u_i}{\partial x_j}-\rho\overline{u_i' u_j'}\right)+F_i$$

$$\tau_{ij} = \rho\overline{u_i' u_j'}$$

Where, u_i is the velocity field in the i direction; ρ is the fluid density; μ is the hydrodynamic viscous coefficient; u_i', u_j' are the pulsation values of the velocity components; p denotes pressure; F denotes the volume force; and τ is the viscous stress.

Two equations are used to describe the turbulent energy (k) and dissipation rate (epsilon), where k represents the turbulent kinetic energy, i.e., the energy possessed by a unit mass of fluid as a result of the turbulent motion. epsilon represents the dissipation rate of turbulent energy, i.e., the rate at which a unit mass of fluid converts turbulent energy into internal energy through viscous action per unit time, and the transport equation is as follows [17]:

$$\frac{\partial(\rho K)}{\partial t} + \frac{\partial(\rho\overline{u_j}K)}{\partial x_j} = \frac{\partial}{\partial x_j}\left[\left(\mu + \frac{\mu_t}{Pr_K}\right)\frac{\partial K}{\partial x_j}\right] + P_K + G_b - \rho\varepsilon - Y_M + S_K$$

$$\frac{\partial\rho\varepsilon}{\partial t} + \frac{\partial(\rho\overline{u_j}\varepsilon)}{\partial x_j} = \frac{\partial}{\partial x_j}\left[\left(\mu + \frac{\mu_t}{Pr_\varepsilon}\right)\frac{\partial\varepsilon}{\partial x_j}\right] + C_{\varepsilon 1}\frac{\varepsilon}{K}(P_K + C_{\varepsilon 3}G_b) - C_{\varepsilon 2}\rho\frac{\varepsilon^2}{K} + S_\varepsilon$$

Where P_K is the generating term for the turbulent kinetic energy K due to the mean velocity gradient; G_b is the generating term for the turbulent kinetic energy K due to buoyancy, and for an unpressurised fluid, $G_b = 0$; $-\rho\varepsilon$ is the dissipation term; Y_M is the compressibility correction term, which is the contribution of pulsatile expansion in compressible turbulence; $C_{\varepsilon 1}\frac{\varepsilon}{K}P_K$ is the generating term for ε; $C_{\varepsilon 1}\frac{\varepsilon}{K}C_{\varepsilon 3}G_b$ is the buoyancy correction term; $-C_{\varepsilon 2}\rho\frac{\varepsilon^2}{K}$ is the dissipation term; S_K and S_ε are the source terms of the K and ε equations, respectively.

A coupled pressure-based solution algorithm is used in this paper, which is different from the separated solution methods such as SIMPLE, SIMPLEC, PISO, etc., the Coupled algorithm achieves the pressure-velocity coupling by solving the continuity equation, momentum equation and energy equation simultaneously.

The wave-making equations are as follows [18-19]:

$$v_h = \zeta_a\omega\frac{chk(z+d_w)}{shkd_w}cosk(x-ct)$$

The vertical velocity equation is:

$$v_v = \zeta_a\omega\frac{shk(z+d_w)}{shkd_w}sink(x-ct)$$

Where ζ_a is the wave amplitude; k is the wave number; ω is the circular frequency; d_w is the water depth; c is the velocity; t is the time.

The wave period is defined as:

$$T = \frac{2\pi}{\omega}$$

The relationship between wave period and wavelength for finite water depth conditions is:

$$T = \left[\frac{g}{2\pi\lambda}tanh\left(\frac{2\pi d}{\lambda}\right)\right]^{-1/2}$$

Where λ denotes the wavelength; g is the gravitational acceleration; T is the wave period.

2.2 Computational model and fluid domain

The computational model in this paper is a 12m aluminium catamaran with the full-scales shown in Table 1, and the material property parameters are shown in Table 2.

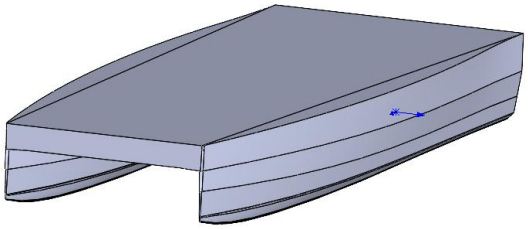

Figure. 1 Computational model

Table 1 Main catamaran measurements

Numble	Parameter	Value	Units
1	Overall length L	12.37	m
2	Breadth B	4.76	m
3	Depth D	1.50	m
4	Draft d	0.56	m
5	Designed displlacement Δ	7.98	t
6	Designed speed v	10.5	m/s

Table 2 Material property

Numble	Parameter	Value	Units
1	Density	2770	kg/m^3
2	Modulus	7.10E+10	Pa
3	Poisson ratio	0.33	
4	Volume modulus	6.96E+10	Pa
5	Shear modulus	2.67E+10	Pa
6	Tensile yield strength	2.80E+08	Pa
7	Compressive yield strength	2.80E+08	Pa
8	Tensile ultimate strength	3.10E+08	Pa

The fluid domain is established by direct stretching, the dimensions are: 75m in the direction of the ship's length, in which the bow is 12m from the inlet, roughly one ship's length, 40m in the direction of the ship's breadth, and 24m in the direction of the ship's depth, in which 12m is below the baseline. Grid encryption is carried out within the range of the ship's perimeter and at the free surface. The final fluid domain is shown in Fig. 2.

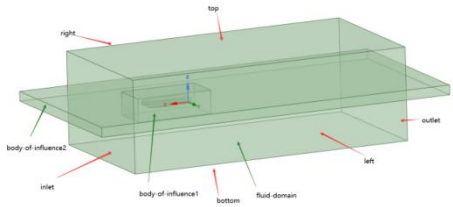

Figure. 2 Fluid domain

This paper investigates the hydrodynamic performance of catamaran in beam waves. The wave height ζ is 0.5m, the wavelengths λ are 4m, 5m, and 6m, respectively, the direction of the waves is 0° to the direction of the catamaran's length, and the speed is 10.5m/s.

2.3 Mesh generation

The majority of the fluid domain is filled with hexahedral cells using the poly-hexcore volume mesh generation method, and polyhedral cells are employed at the wall and in close proximity to the ship's surface to create a common node connection between the two mesh types. Within one wave height, there are no fewer than 10 mesh amounts taking into account, the number of the body mesh is 188,664,000, and the mesh generation is displayed in Fig. 3.

Adaptive grids are used to divide the frame grids, to guarantee two layers of cells at least, the smallest size in the frame is served as the base grid size. The maximum cell size is set to 20mm, and the number of poorest grids is kept below 5%, so as to ensure the accuracy and validity of the

calculation. There are 654,000 nodes and 629,000 cells, the frame and hull surface mesh are shown in Fig. 4.

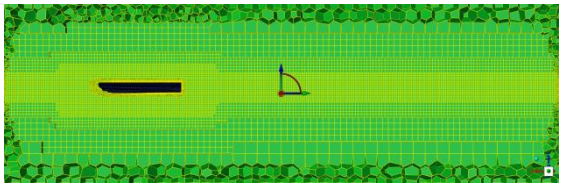

Figure. 3 Fluid domain mesh

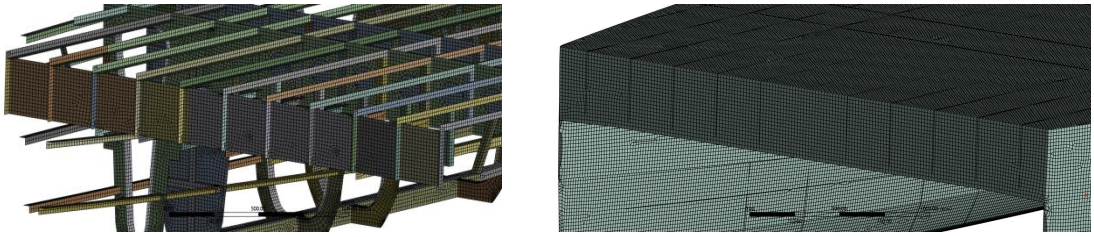

(a) Frame mesh (b) Hull surface mesh

Figure. 4 Frame and hull surface mesh

3. Results and analyzes

3.1 Constraint and solution setup

Considering that the ship is subject to wave force, gravity, buoyancy and other loads when sailing on the surface of the water, these loads are simplified to the total pressure on the surface of the ship and its own gravity, of which the total pressure is divided into static and dynamic pressure. Because ship is in a dynamic equilibrium and has the periodic acceleration under the ideal wave action, to prevent the large rigid body displacement during the calculation, "321" constraint method is used. Two displacement constraints are added at the bow and stern of the center longitudinal plane on the main deck, the bow point constrains the displacement of the three directions of x, y and z, and the stern point constrains the displacement of y and z. The third restraining point is at the stern of the center longitudinal on the orlop, restraining the displacement in y direction. The details of the constraint points are shown in Fig. 5.

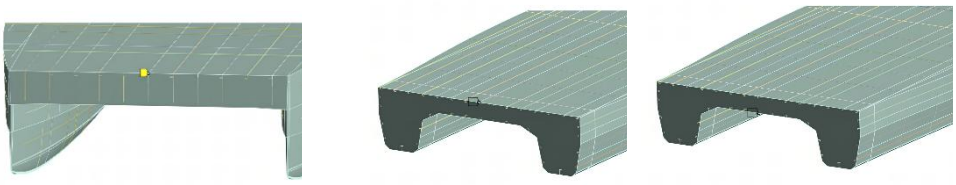

(a) (b) (c)

Figure. 5 Constraint setup

3.2 Results

Fig. 6 below shows the duration and residual curves of total pressure, static pressure and dynamic pressure at different wavelengths. Where tp represents the total pressure, sp represents the static pressure and dp represents the dynamic pressure. It can be seen from the duration curves that different pressure curves at different wavelengths show periodic variation characteristics, and the curves are oscillated smooth, without sudden jumps and attenuation phenomena. The residual curves also show obvious periodic oscillation changes, which indicates that the pressure of the hull can be calculated and analyzed based on the solution method. Fig. 7 shows the free surface at three beam wavelengths, it can be seen that in the transverse range, the beam wave is regular periodic, the wave height of the left and right sides of the hull are similar, and there is no obvious wave

attenuation, which indicates that the transverse wave established is effective, so it can be carried out the structural finite element analysis on the high-speed catamaran.

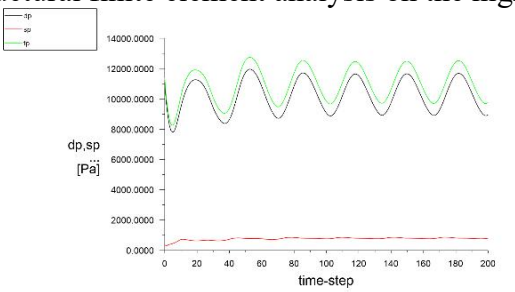

(a) λ=4m durantion curve

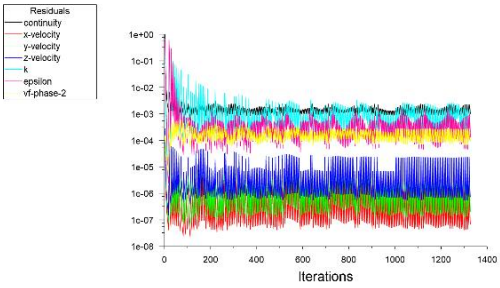

(b) λ=4m residual curve

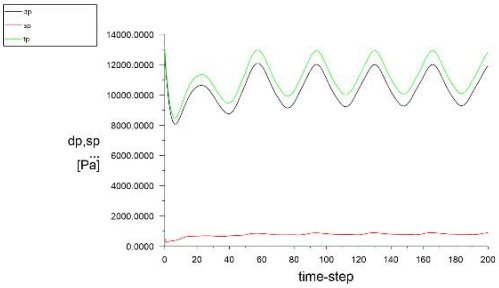

(c) λ=5m durantion curve

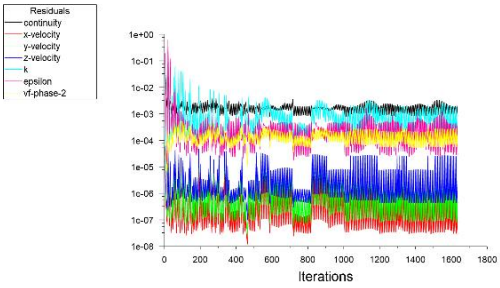

(d) λ=5m residual curve

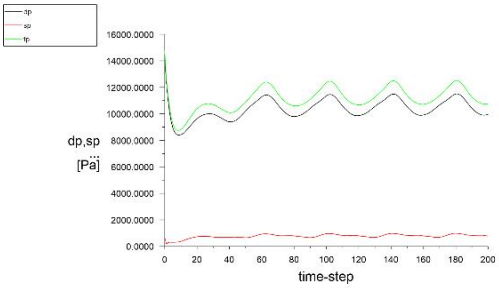

(e) λ=6m durantion curve

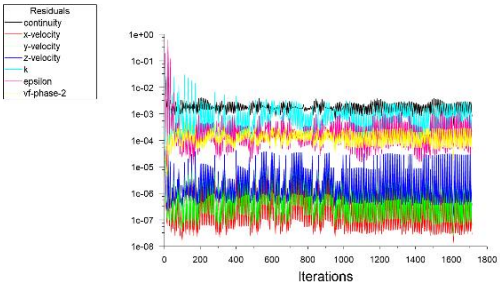

(f) λ=6m residual curve

Figure. 6 Duration and residuals curves at different wavelengths

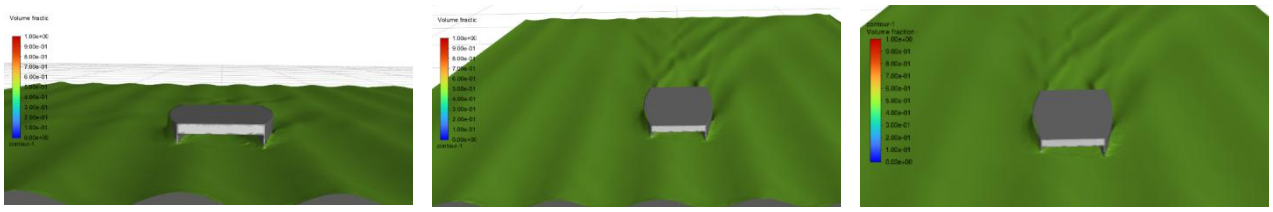

(a) λ=4m (b) λ=5m (c) λ=6m

Figure. 7 Free surface at different wavelengths

Fig. 8 shows the maximum deformation at the pressure peak and trough for the three wavelengths. The maximum deformation gradually increased at the pressure peak with the wavelength increasing, the maximum deformation is 4.651mm at the 6m wavelength. While at the pressure trough, the maximum deformation is 4.157mm at λ/L = 0.42, the curve first increases and then decreases. Fig. 9 shows the average deformation at the pressure peak and trough for the three wavelengths. Both curves increase as the wavelength increase. Fig. 10 shows the maximum equivalent stress at the pressure peak and trough for the three wavelengths. The maximum equivalent stress gradually increased at the pressure peak with the wavelength increasing, the maximum equivalent stress is 115.42Mpa at the 6m wavelength. While at the pressure trough, the

maximum equivalent stress is 102.73Mpa at λ/L = 0.42, the curve first increases and then decreases. Fig. 11 shows the maximum shear stress at the pressure peak and trough for the three wavelengths. The maximum shear stress gradually increased at the pressure peak with the wavelength increasing, the maximum shear stress is 65.648Mpa at the 6m wavelength. While at the pressure trough, the maximum shear stress is 58.388Mpa at λ/L = 0.42, the curve first increases and then decreases.

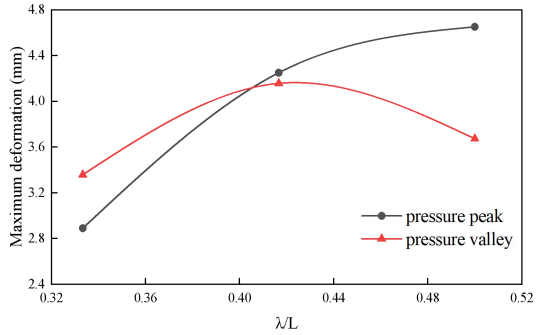

Figure. 8 Maximum deformation at different wavelengths and pressures

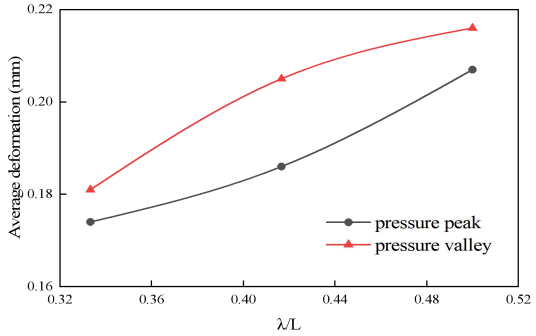

Figure. 9 Average deformation at different wavelengths and pressures

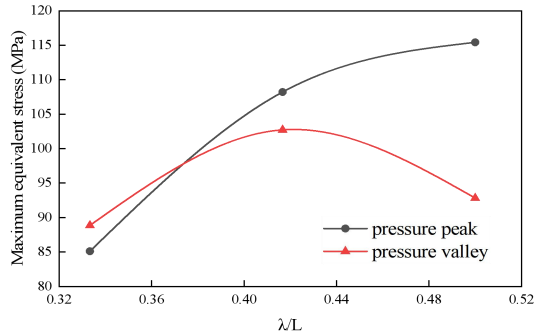

Figure. 10 Maximum equivalent stress at different wavelengths and pressures

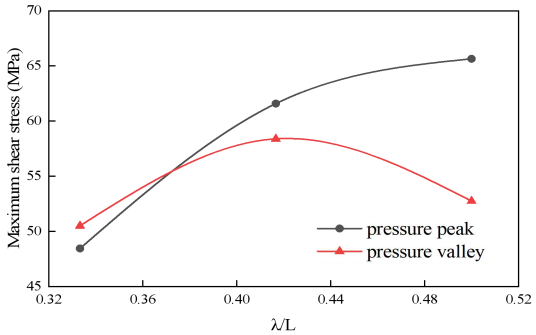

Figure. 11 Maximum shear stress at different wavelengths and pressures

Fig. 12 shows the stress-deformation diagram at different wavelengths, in which the left diagram is deformation and the right diagram is stress. It can be seen that under the action of beam waves, the stress on the left and right side of the catamaran deck are not uniform and distributed asymmetrically, the incoming side has a greater impact on the hull. The hull has obvious deformation when the wavelength is 5m. The pressure difference at the stern is closer in different wavelengths, while there is a more obvious difference at the bow, which indicates that the wave load has a greater influence on the bow of the catamaran compared to the stern, which is related to the structural design of the bow.

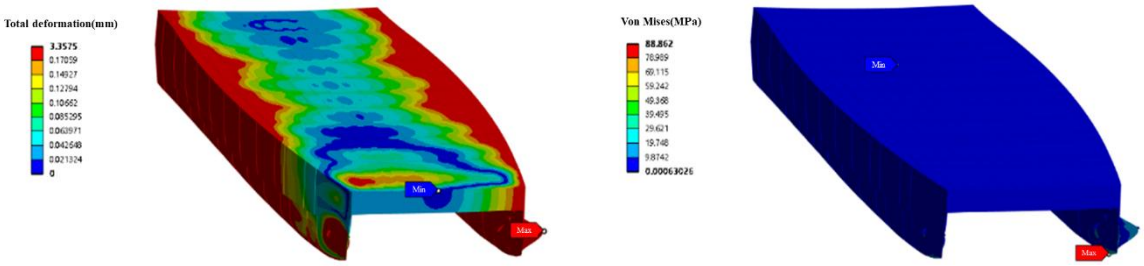

(a) λ=4m

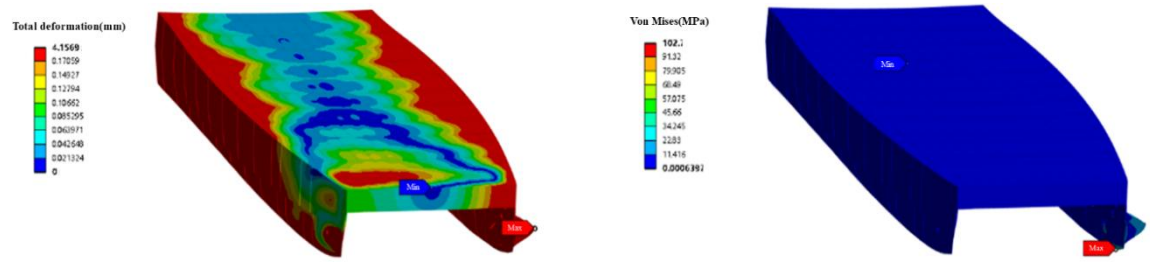

(b) λ=5m

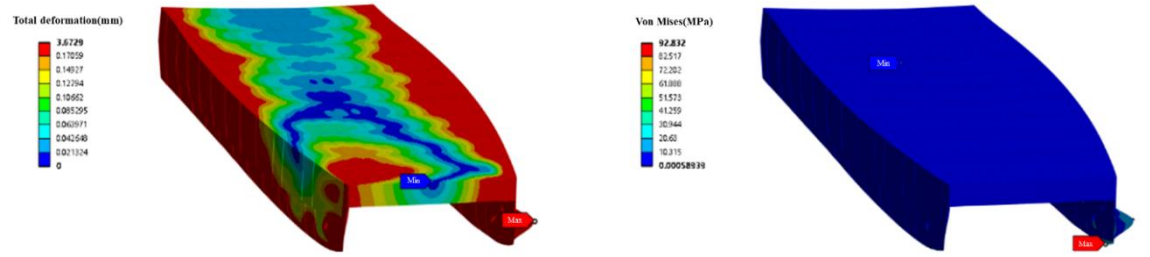

(c) λ=6m

Figure. 12 Stress-deformation diagram at different wavelengths

3.3 Structural optimisation and analysis

Base on the stress-deformation characteristics of the catamaran in beam waves, to strengthen the structure, the hull structure is optimized, both bow and stern of the hull add a transverse frame, the bow stiffeners extend to the keel.

Fig. 13-Fig. 16 show the stress- deformation curves at different wavelengths and pressures after optimization. It can be seen that after optimization, the maximum deformation of the hull structure is significantly reduced with a maximum reduction of 46.45%. The average deformations are also significantly reduced compared to the pre-optimization. This indicates that increasing frame can significantly resist the impact of beam wave loads and guarantee the structural safety of the catamaran. Fig. 17 shows the stress-strain diagram under the action of beam waves after structural optimization. It can be clearly indicated that, the large deformation areas are greatly reduced. Fig. 18 shows the deformation comparison of the stern hull, the deformation areas are also greatly reduced.

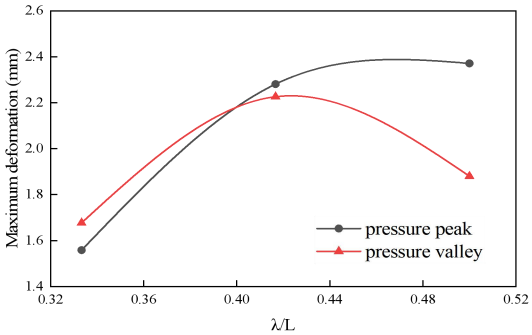

Figure. 13 Maximum deformation at different wavelengths and pressures

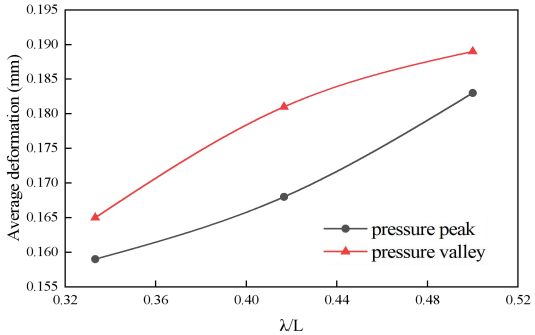

Figure. 14 Average deformation at different wavelengths and pressures

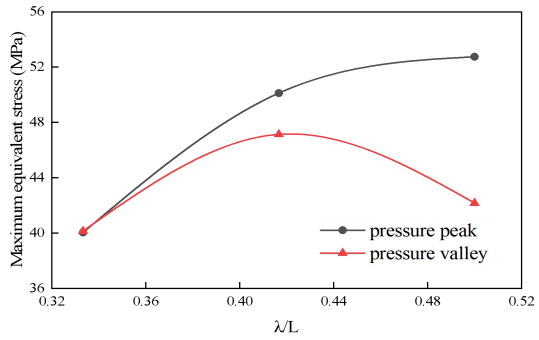

Figure. 15 Maximum equivalent stress at different wavelengths and pressures

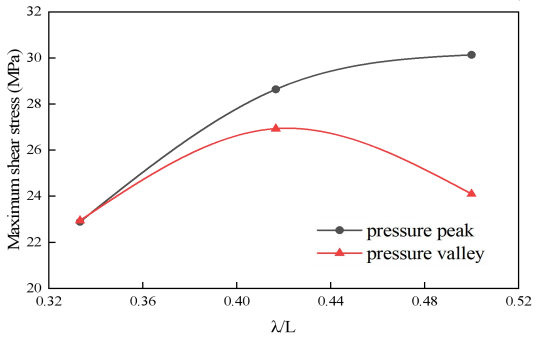

Figure. 16 Maximum shear stress at different wavelengths and pressures

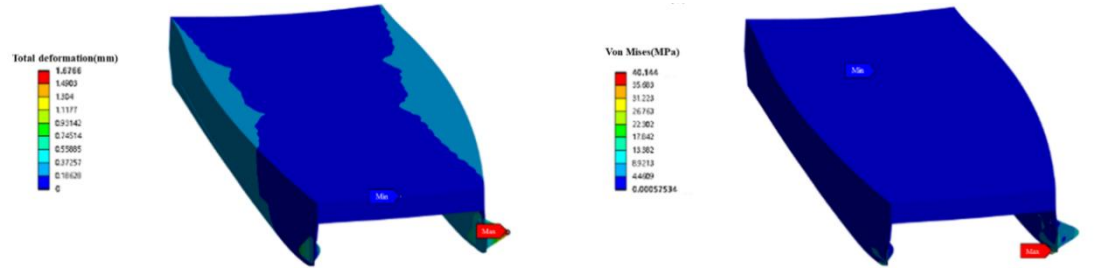

(a) λ=4m

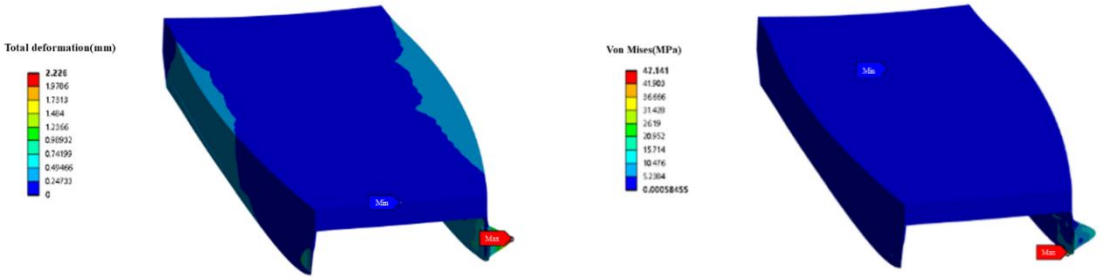

(b) λ=5m

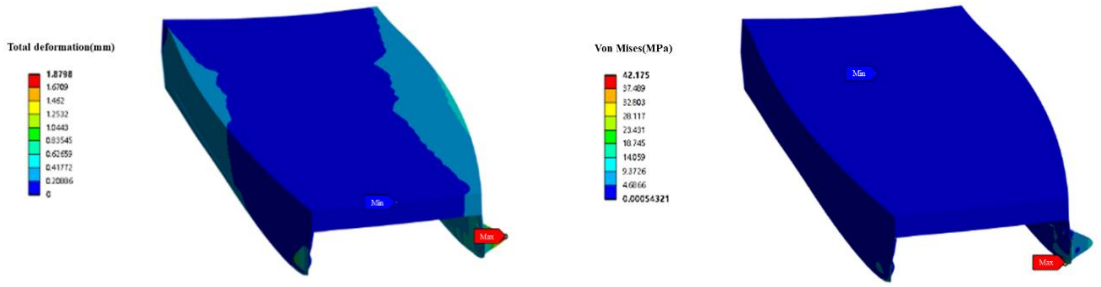

(c) λ=6m

Figure. 17 Stress-deformation diagram at different wavelengths

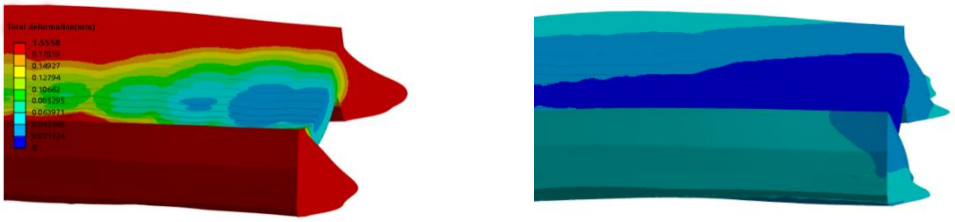

(a) Before optimization (b) After optimization

Figure. 18 Deformation comparison of the stern hull

4. Summary

This paper used CFD and FEA methods to study the stress-strain characteristics of catamaran under the action of beam waves in high-speed, carried out structural optimization, and obtained the following conclusions:

(1) Beam waves are established by FLUENT, there is no wave attenuation in the direction of the ship width, and the numerical tank can be applied to the finite element analysis of the catamaran structure.

(2) When the catamaran encounters beam waves, the wave load on the facing side of the wave direction is larger, so that the deformation of the bow is larger compared with the stern, and the characteristic of maximum deformation of the hull is basically the same as the maximum equivalent stress.

(3) Through the transverse structural reinforcement and the stiffener extension, the overall structural strength of the hull can be effectively improved and the structural deformation of the hull can be reduced. The structural optimization of this paper makes the maximum deformation of the catamaran in high-speed sailing state reduced by 46.45%.

References

[1] LI Yunbo, FU Zheng, GONG Jiaye, DAI Kun etal. Research on Rolling Stability of Trimaran in Beam Waves. China Shipbuilding, 2021,62(4): 89-100. (in Chinese)

[2] Xu Zhouyuan. The Research of the Coupled Movement of Two Ships Under Wave Action. Dalian Maritime University, 2021. (in Chinese)

[3] CHEN Jiong, YANG, Qi. Case study of transverse strength calculation of cargo ship under the load of transverse wave. China water transport, 2023,9: 71-73. (in Chinese)

[4] LI Huailiang, YU Wentai, LI Xinchao, BAI Xiaodong. Experimental investigation on dynamic response characteristics of the twin barge float – over installation of mega topsides in beamwaves. China Offshore Oiland Gas, 21, 33 (2): 172-179. (in Chinese)

[5] LU Weiwei, LI Shu- jun, YU Shen- guang, SONG Lan- fang. Dynamic mooring and impact force of tugboats under beam seas. Port & Waterway Engineering, 2022, 597(7):81-86. (in Chinese)

[6] TU Jianjun, FENG Feng, JIA Linnan. Local Strength Analysis of Planning Boat Based on Fluid-Structure Interaction. SHIPBUILDING OF CHINA, 2023，64(5):86-97. (in Chinese)

[7] TIAN Xiaojie， XIE Dashuai， LIU Guijie， XIE Yingchun. Analysis of fluid-structure interaction characteristics of gas-liquid two-phase flow marine riser based on ANSYS. JOURNAL OF VIBRATION AND SHOCK, 2021, 40(7): 260-267. (in Chinese)

[8] Ying T, Shi-Li S, Arash A. A fully nonlinear BEM-beam coupled solver for fluid – structure interactions of flexible ships in waves. Journal of Fluids and Structures, 2023, 121.

[9] Yun Yajie. Strength analysis of the whole ship based on fluid-structure coupling. Dalian Maritime University, 2024. (in Chinese)

[10] Zhou Zhilu. Research on the Fluid-Structure Coupling Characteristics of Large-scale Flexible Blade Wind Turbine. Harbin Engineering University.2022. (in Chinese)

[11] LEI xiaoshan, MA yong, LIN shijie. Numerical Simulationon Aerodynamic Performance of a Sail Wing at Different Wind Speeds Based on Unidirectional Fluid-Structure Interaction. Journal of Wuhan Institute of Physical Education, 2019, 53(11):95-100. (in Chinese)

[12] Meng Chaoping, Ma Jianlong, Lv Wenchun. Research on calculation method of dynamic mode of wind turbine based on one-way FSI. Renewable Energy Resources, 2016, 34(6): 884-888. (in Chinese)

[13] Du Zixue, Han Shanhe1, Liu Yaqian. Strength and Vibration of One-Way Fluid-Solid Coupling Turbocharger Impeller. JOURNAL OF CHONGQING JIAOTONG UNIVERSITY (NATURAL SCIENCE), 2014, 33(2): 142-145. (in Chinese)

[14] AN Bang, ZHANG Hemu, ZHU Hanhua1. Numerical Comparison Analysis of Propeller Performance Based on Fluid Solid Coupling[J]. MACHINE TOOL & HYDRAULICS, 2018, 46(17): 155-160. (in Chinese)

[15] Specification for Classification and Construction of Offshore High Speed Vessels. China Classification Society.2022. (in Chinese)

[16] CHEN Ping, GUAN Yanmin, YU Qiancheng, et al. Numerical simulation of propeller loads on ships navigating in broken ice. Ship Science and Technology, 2023, 45(8):15-19. (in Chinese)

[17] Tao Yihan. Research on ship wave force modeling in regular waves based on CFD. Dalian Maritime University,2014. (in Chinese)

[18] Wang YuFan. Development of ship structure program based on inertial release principle. South China University of Technology,2022. (in Chinese)

[19] Pei ZY, Chen W, Yang P, Wu WG. Strength and structural design of ship hull. Beijing: Science Press, 2017:43. (in Chinese)